High Permeability and Low Core Losses of Nanocrystalline Fe-Nb-Zr-B-Cu Alloys

Sci. Rep. RITU A42 (1996) pp. 121-125
No. 1, March 1996

High Permeability and Low Core Losses of Nanocrystalline Fe-Nb-Zr-B-Cu Alloys*

A. Makino[1], T. Hatanai[1], S. Yoshida[1], N. Hasegawa[1], A. Inoue[2] and T. Masumoto[2]

[1] *Nagaoka Branch, Central Research Laboratory, Alps Electric Co.,Ltd., Nagaoka 940, Japan*

[2] *Institute for Materials Research, Tohoku Univ., Sendai 980, Japan*

(Received December 5, 1995)

Nanocrystalline Fe-M-B (M=Zr or Nb) alloys prepared by crystallization of rapidly quenched amorphous ribbons are known as a new class of soft magnets with high saturation magnetization. In order to improve their soft magnetic properties further, the reduction of their magnetostriction to zero was attempted by a combined addition of Zr and Nb, because the signs of the magnetostriction of the Fe-Zr-B and the Fe-Nb-B at each optimum condition are known to be opposite. Further, the B concentration was reinvestigated under a Cu addition and the combined addition of Zr and Nb in order to further refine the grain size and to improve the intergranular exchange coupling. As a result, the small average grain size of 8nm and nearly zero magnetostriction has been simultaneously obtained in the $Fe_{84}Nb_{3.5}Zr_{3.5}B_8Cu_1$ alloy. This alloy simultaneously exhibits the high permeability of 100,000 (at 1kHz) and the high saturation flux density of 1.53T, satisfying the both properties in the highest level among the rapidly quenched ribbons ever reported. The core losses of the nanocrystalline $Fe_{84}Nb_{3.5}Zr_{3.5}B_8Cu_1$ alloy are lower than those of the amorphous Fe-Si-B alloys over a wide frequency and B_m (maximum induction) range. Further, the core losses are almost unchanged under the stresses such as epoxy resin molding. These new nanocrystalline materials are suitable for use in advanced electronic devices such as inductors or transformers.

KEYWORDS: nanocrystalline, soft magnetic alloy, melt spun ribbon, amorphous alloy, crystallization, core loss

1. Introduction

Recently, development of new soft magnetic materials with higher performance is strongly desired along with the progress and miniaturization of electronic devices such as inductors or transformers. As a candidate of such materials, nanocrystalline Fe-Si-B-Nb-Cu[1] or Fe-P-C-Ge-Cu[2] alloys produced by annealing the melt-spun amorphous ribbons are known to posses high permeability. However, the saturation flux density of such alloys is substantially lower than that of conventional iron-based amorphous alloys because the composition of these alloys is based on the typical metal-metalloid amorphous alloys, such as Fe-Si-B or Fe-P-C, and contains the other non-magnetic additional elements such as Cu, Nb or Ge. On the other hand, authors found that Cu-free Fe-M-B (M=Zr, Nb, Hf) alloys nanocrystallized from amorphous state simultaneously exhibit high saturation flux density B_s of 1.6-1.7T and high permeability[3]-[5]. The high B_s of these alloys is due to the less metalloid concentration than in the above-mentioned alloys. It was also shown that the bcc grain size is further reduced by a small addition of Cu, leading to a further increase of permeability[4][5]. The magnetostriction of Fe-Nb-B and Fe-Nb-B-Cu alloys is positive whereas that of Fe-Zr-B and Fe-Zr-B-Cu alloys is negative, around the optimum composition for soft magnetic properties for each alloy. Though these magnetostriction is sufficiently small, of the order of 10^{-6}, further improvement of magnetic softness is expected by further reduction of magnetostriction.

In the present investigation, high permeability more than 100,000 (at 1kHz) was attained maintaining the high B_s of 1.5T in an attempt to obtain zero magnetostrictive alloys by a combined addition of Nb and Zr, and by controlling the B concentration.

2. Experimental procedure

Fe-M-B and Fe-M-B-Cu (M=Zr and/or Nb) alloy ribbons were produced by a single-roller melt spinning method in an argon atmosphere. The width and thickness of the ribbons were 14.5mm and approx. 20μm, respectively. The alloy compositions are nominally expressed in atomic per cent.

The melt-spun ribbons were heat-treated at a heating rate of 3K/s in an evacuated state.

Measurements of effective permeability μ_e, coercivity H_c, and core loss W were performed with a ring-shaped specimens, prepared by mechanical punching, with a size of 6mm in inner diameter and 10mm in outer diameter. The μ_e was measured by an impedance analyzer at 1kHz under a field of 0.4A/m. A dc B-H tracer and an ac B-H analyzer operated under the sinusoidal magnetization were used to measure the H_c and the W, respectively. Saturation flux density B_s and temperature dependence of saturation

*IMR, Report No. 2018

magnetization σ_s was evaluated by a vibrating sample magnetometer (VSM) under 800kA/m. Magnetostriction λ_s was measured by a strain gauge technique or by a change in an anisotropy energy ΔE (evaluated from magnetization curve) before and after encapsulating the ring-shaped specimen with epoxy resin (molding the resin with the specimen). In the latter method, the λ_s is calculated by

$$\Delta E = -(3/2)\lambda_s \cdot \sigma \qquad (1)$$

where σ is a stress induced by a solidification of resin. In this method, stress-induced anisotropy is assumed to be in-plane or perpendicular to the plane depending on the sign of λ_s. The σ was calibrated by the sample with known λ_s value measured by the strain gauge.

The alloy phase was identified with an X-ray diffractometry using Co-Kα radiation. Average grain size D was evaluated from the half-maximum breadth of $\{110\}_{bcc}$ reflection peak using Scherrer's equation. Microstructure was observed by a 200kV transmission electron microscope (TEM).

3. Results and discussion

In the nanocrystalline Fe-Zr-B and Fe-Nb-B alloys, the composition region where the permeability shows its maximum value does not strictly coincides with the zero-magnetostriction line as mentioned above[6]. The best soft-magnetic properties are attained around the compositions of $Fe_{90}Zr_7B_3$ and $Fe_{84}Nb_7B_9$. Since the magnetostriction changes from negative to positive with increasing B concentration for both the alloys, the λ_s of the $Fe_{90}Zr_7B_3$ alloy is negative whereas that of the $Fe_{84}Nb_7B_9$ alloy is positive. This relation is holds for the alloys containing 1at% Cu. By a combined addition of Zr and Nb and balancing their ratio and B concentration, the composition where the zero magnetostriction and the highest permeability are simultaneously obtained was investigated.

At first the Zr, Nb, and B concentrations were investigated by choosing $Fe_{89}Zr_7B_3Cu_1$ and $Fe_{83}Nb_7B_9Cu_1$ as basic constituents and mixing them in various ratios. Figure 1 shows the composition dependence of Bs, Hc, μ_e(at 1kHz), λ_s, and D. The abscissa of the figure is a parameter expressing the ratio of the $Fe_{83}Nb_7B_9Cu_1$ constituent. For example, the over-all alloy composition is $Fe_{89}Zr_7B_3Cu_1$ when the parameter is zero, and $Fe_{83}Nb_7B_9Cu_1$ when it is one. As can be seen in the figure, the Bs, λ_s, and D are continuously and monotonically changing. The Hc and μ_e take their minimum and maximum, respectively, at the composition where the λ_s goes through zero, as expected.

To further optimize the alloy composition, B concentration and Zr/Nb ratio were precisely investigated around the composition of $Fe_{86}Nb_{3.5}Zr_{3.5}B_6Cu_1$ where the best soft magnetic properties were obtained in Fig.1. Figure 2

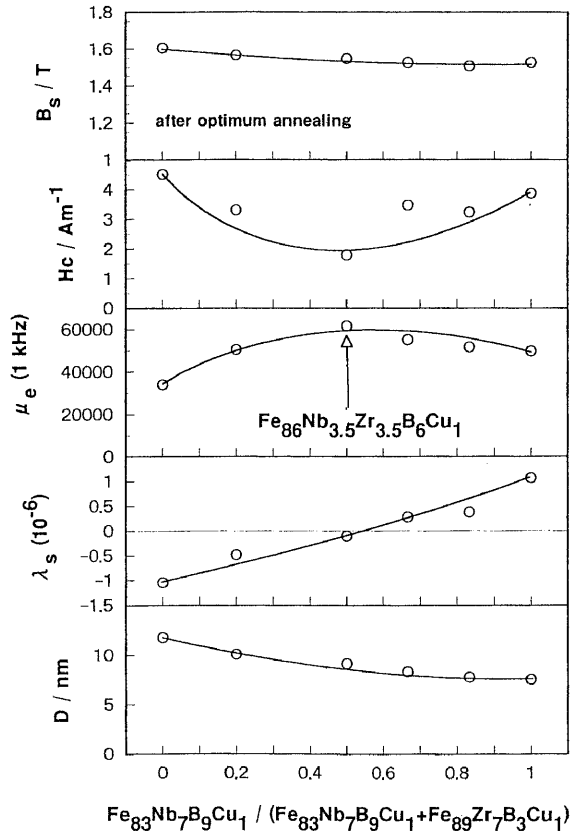

Fig.1 Composition dependence of saturation flux density Bs, coercivity Hc, effective permeability μ_e(at 1kHz), magnetostriction λ_s, and average grain size D for nanocrystalline Fe-Nb-Zr-B-Cu alloys.

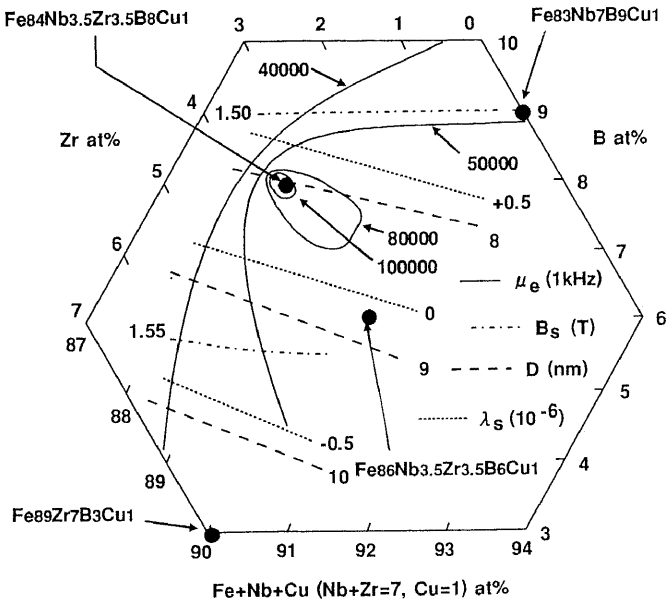

Fig.2 Pseudo-ternary diagram of saturation flux density Bs, effective permeability μ_e(at 1kHz), magnetostriction λ_s, and average grain size D for the (Fe-Nb-Cu)-Zr-B alloy after annealing at the optimum conditions.

shows the pseudo-ternary diagram of magnetic properties and grain size, where the Nb+Zr and Cu concentrations were kept at 7at% and 1at%, respectively. The λ_s and D are dependent on both the B concentration and the Zr/Nb ratio whereas the B_s is mainly dependent on the Fe concentration. The best soft magnetic properties are obtained at the $Fe_{84}Nb_{3.5}Zr_{3.5}B_8Cu_1$ which is more B-rich than the line linking the point of the $Fe_{89}Zr_7B_3Cu_1$ to the $Fe_{83}Nb_7B_9Cu_1$ in the figure. It was found that the high permeability of 100,000 as well as the B_s of 1.53T was obtained simultaneously at that composition.

In Fig.3, X-ray diffraction patterns of the $Fe_{84}Nb_{3.5}Zr_{3.5}B_8Cu_1$ alloy are shown. A halo pattern which is an indication of amorphous state is seen in an as-quenched state. After annealing at 833K for 1.8ks, broad diffraction peaks of bcc-Fe phase are seen. The fine bcc grains with 8nm in mean grain size are homogeneously distributed as seen in the bright-field TEM image of this alloy (Fig.4). Though such microstructure is quite similar to that of the Fe-M-B alloys, the grains are further refined in this alloy..

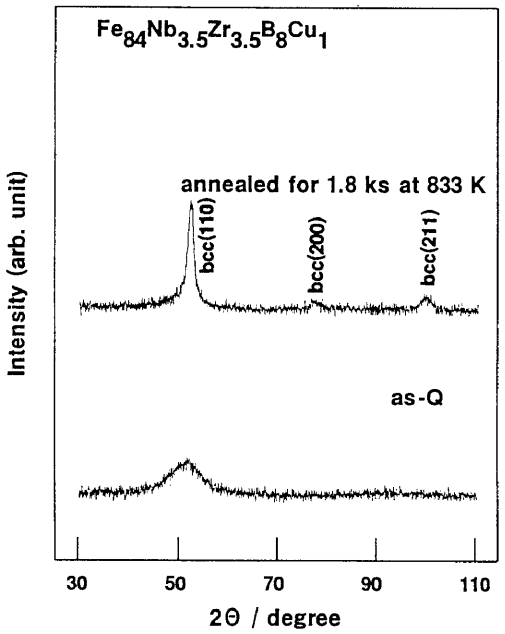

Fig.3 X-ray diffraction patterns of $Fe_{84}Nb_{3.5}Zr_{3.5}B_8Cu_1$ alloy in an as-quenched state and after annealing at 833K for 1.8ks.

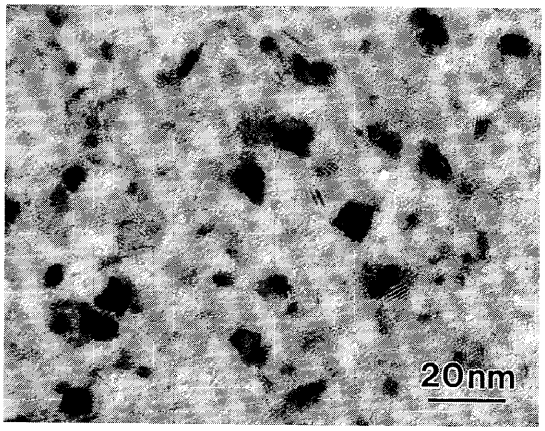

Fig.4 Bright-field TEM image of $Fe_{84}Nb_{3.5}Zr_{3.5}B_8Cu_1$ alloy annealed at 833K for 1.8ks.

To further explain the excellent soft magnetic properties of the $Fe_{84}Nb_{3.5}Zr_{3.5}B_8Cu_1$ alloy, some important factors such as magnetostriction and grain size as well as intergranular magnetic coupling were further discussed. Figure 5 shows the relation between the mean grain size and the magnetostriction. Various Fe-M-B and Fe-M-B-Cu alloys are plotted and contour lines of μ_e are drawn in the figure. In Fe-Zr-B alloys, grain size less than 10nm is not attained though the grains become small by the Cu addition. In Fe-Nb-B alloys, on the other hand, magnetostriction increases its positive value though the grains are refined to 8nm by the Cu addition. It is also seen from the figure that both the magnetostriction and the grain size are minimized by controlling the B concentration and a combined addition of Zr and Nb. The region where the μ_e takes its maximum does not strictly coincide with the zero-magnetostrictive region but is slightly shifted toward positive side. The one reason considered is the rather dominant effect of the grain size than that of the magnetostriction, because the smaller grain size tends to be obtained in the positive-λ_s side.

Another reason considered is concerning the strength of exchange coupling between bcc nanograins. This inter-

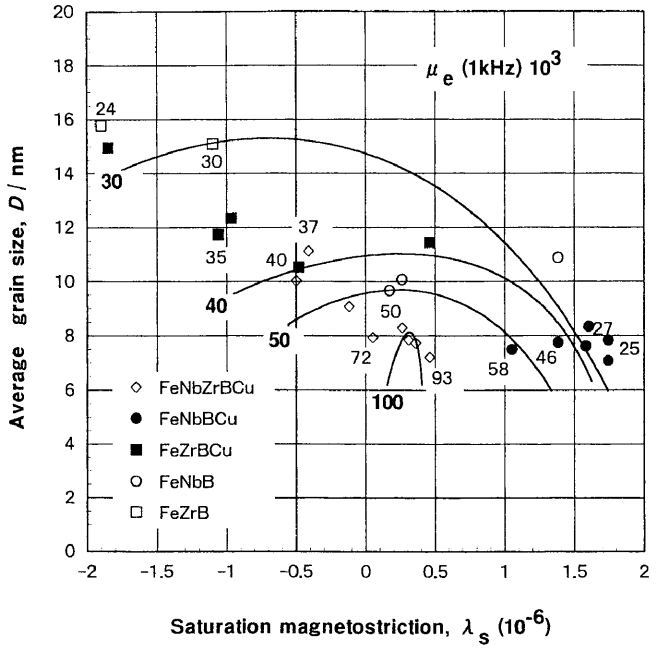

Fig.5 Relation between average grain size D and magnetostriction λ_s together with the contour lines of effective permeability μ_e(at 1kHz) for nanocrystalline Fe-M-B and Fe-M-B-Cu (M=Zr and/or Nb) alloys.

granular coupling works to align the magnetization of adjacent grains and averages out the magnetocrystalline anisotropy[7]. In the Fe-M-B and Fe-M-B-Cu alloys, the intergranular coupling is mediated by a residual amorphous phase surrounding the bcc nanograins[4]. When the Curie temperature of the residual amorphous phase is low, it can not fully mediate the intergranular interaction owing to the thermal fluctuation of the spins inside the amorphous phase. Since the Curie temperature of amorphous Fe-M-B phase goes up as the B concentration increases[8], the intergranular coupling is speculated to become stronger in the composition region where the B concentration of the residual amorphous phase becomes higher. Figure 6 shows the temperature dependence of the square of the saturation magnetization σ_s of the $Fe_{83}Nb_7B_9Cu_1$, $Fe_{89}Zr_7B_3Cu_1$, and $Fe_{84}Nb_{3.5}Zr_{3.5}B_8Cu_1$ alloys annealed at 773K for 1.8ks. Curie temperature of the residual amorphous phase $T_c(amo.)$ was evaluated from the inflection points of the σ_s^2-T curves †. Though the $T_c(amo.)$ is not in a simple relation with the over-all B concentration, the highest $T_c(amo.)$ is observed in the most soft magnetic $Fe_{84}Nb_{3.5}Zr_{3.5}B_8Cu_1$ alloy. Therefore the higher $T_c(amo.)$, that is the stronger intergranular coupling, will be also responsible for the appearance of the highest μ_e region in Fig.5. The best soft magnetic region in the present alloys is probably resulted from a counterbalance of the grain size, magnetostriction, and the intergranular magnetic coupling.

Since the $Fe_{84}Nb_{3.5}Zr_{3.5}B_8Cu_1$ alloy has nearly zero magnetostriction, excellent performance is expected even under the stress such as that after a resin molding (encapsulating). Figure 7 shows the frequency characteristics of core losses W measured at maximum induction Bm of 0.2T before and after the epoxy resin molding. The stress applied to the specimen from the resin used in this test was approx. 140MPa which is compressive. In Fig.7, the characteristics of an amorphous Fe-Si-B alloy annealed at an optimum condition are also shown for comparison. The core losses of the $Fe_{84}Nb_{3.5}Zr_{3.5}B_8Cu_1$ alloy are 1/3~1/4 of those for the amorphous Fe-Si-B alloy over a wide frequency range from 10kHz to 500kHz. Moreover the low core losses of the $Fe_{84}Nb_{3.5}Zr_{3.5}B_8Cu_1$ alloy are almost unchanged under the stresses.

† For the linear relation, the exponent of 3 is generally used according to the constant coupling approximation[9] rather than the 2 according to the molecular field approximation. On the other hand, the exponent of 1/0.36 is reported to fit well with the experimental results over a wide temperature range from room temperature to T_c[10]. However, the exponent of 2 was used because the present results showed better fit by using the 2 rather than by using the 3 or the 1/0.36.

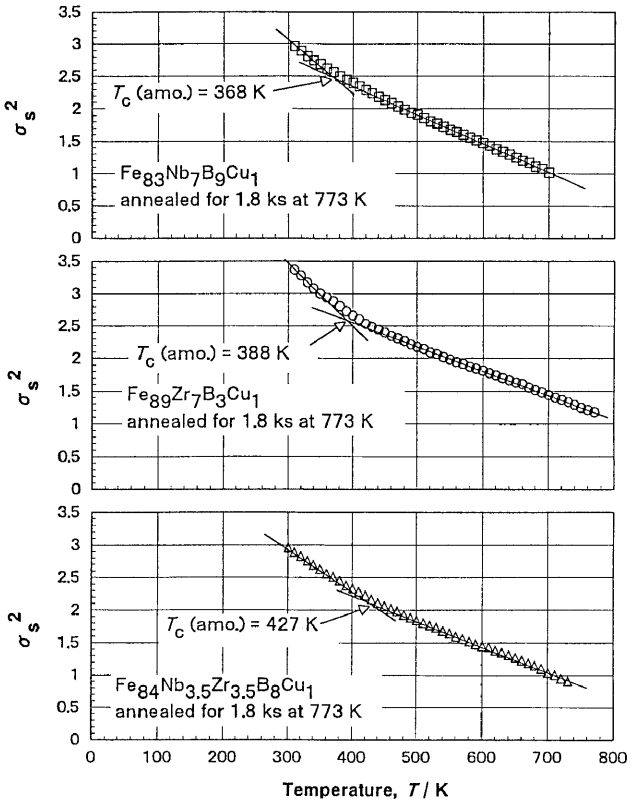

Fig.6 Temperature dependence of the square of the saturation magnetization σ_s of the $Fe_{83}Nb_7B_9Cu_1$, $Fe_{89}Zr_7B_3Cu_1$, and $Fe_{84}Nb_{3.5}Zr_{3.5}B_8Cu_1$ alloys annealed at 773K for 1.8ks.

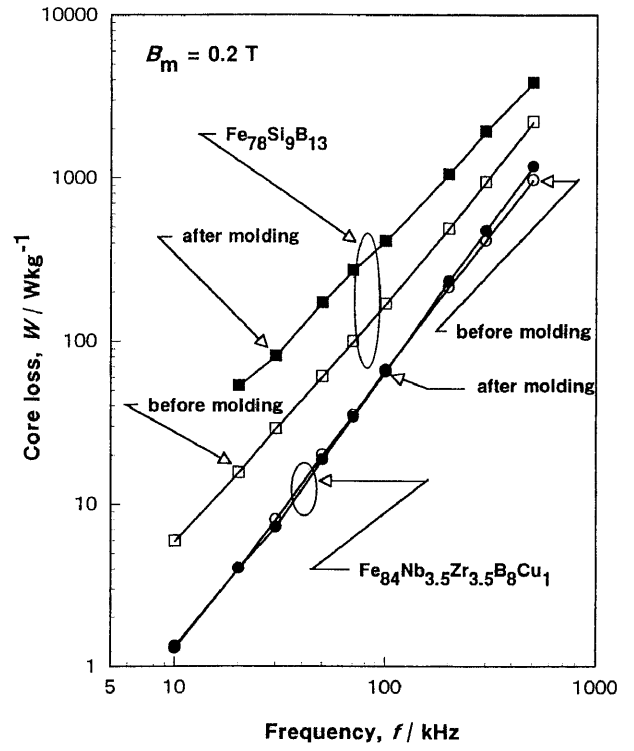

Fig.7 Relation between core losses at 0.2T and the frequency for nanocrystalline $Fe_{84}Nb_{3.5}Zr_{3.5}B_8Cu_1$ alloy before and after the epoxy resin molding. The data for amorphous $Fe_{78}Si_9B_{13}$ alloy are also shown for comparison.

Figure 8 shows the *Bm* dependence of the core losses at 50Hz for the nanocrystalline Fe84Nb3.5Zr3.5B8Cu1 alloy, the amorphous Fe-Si-B alloy ,and a grain oriented silicon steel. The core losses of the Fe84Nb3.5Zr3.5B8Cu1 alloy are lower than those of the amorphous Fe-Si-B alloy and the grain oriented silicon steel in a wide *Bm* range from 0.2T to 1.4T. Thus the nanocrystalline Fe84Nb3.5Zr3.5B8Cu1 alloy shows the excellent core performance in the high *Bm* region at the commercial frequency.

Table 1 summarizes the magnetic properties of the nanocrystalline Fe84Nb3.5Zr3.5B8Cu1 alloy together with the other soft magnetic alloys. The effective permeability of the Fe84Nb3.5Zr3.5B8Cu1 alloy is the highest among the nanocrystalline Fe-M-B alloys ever obtained. It is concluded that the alloy developed in the present investigation simultaneously possesses the highest saturation flux density and the best soft magnetic properties among the rapidly quenched ribbons ever reported.

4. Conclusion

To improve the soft magnetic properties of Fe-M-B alloys, Cu addition and a combined addition of Zr and Nb as well as an optimization of B content was made. The results are summarized as follows:

(1) The small average grain size of 8nm and nearly zero magnetostriction of the order of 10^{-7} is simultaneously obtained in the Fe84Nb3.5Zr3.5B8Cu1 alloy.

(2) The Fe84Nb3.5Zr3.5B8Cu1 alloy shows the high saturation flux density of 1.53T and high permeability of 100,000.

(3) The microstructure of the Fe84Nb3.5Zr3.5B8Cu1 alloy consists mostly of ultrafine bcc phase similarly to the other Fe-M-B (M=Zr, Hf, Nb) alloys.

(4) The core losses of the nanocrystalline Fe84Nb3.5Zr3.5 B8Cu1 alloy are lower than those of the amorphous Fe-Si-B alloys over a wide frequency and *Bm* range. Further the core losses are almost unchanged under the stresses.

Acknowledgements

The authors would like to thank Mr. K. Oominato of Alps Electric Co., Ltd. for his technical assistance in TEM observations.

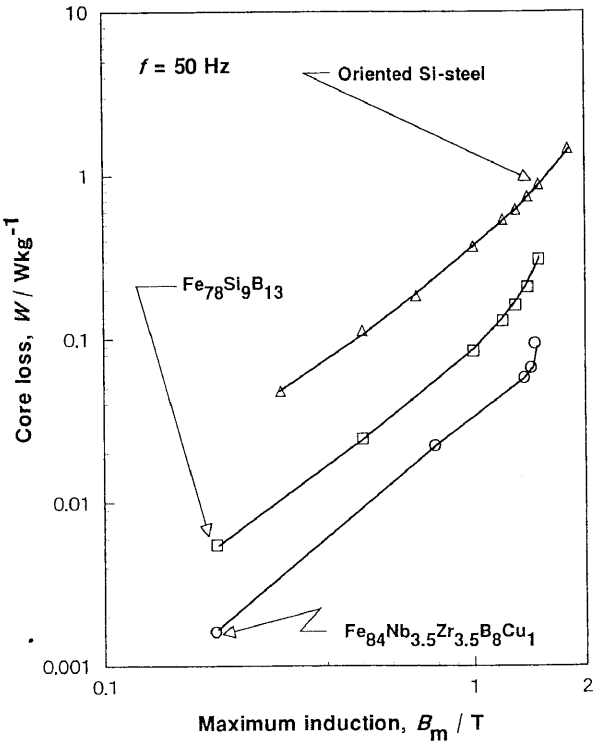

Fig.8 Relation between core losses at 50Hz and maximum induction for nanocrystalline Fe84Nb3.5Zr3.5B8Cu1 alloy. The data for amorphous Fe78Si9B13 alloy and grain oriented silicon steel are also shown for comparison.

Table 1 Magnetic properties of nanocrystalline Fe-Nb-Zr-B-Cu alloy and other soft magnetic alloys.

Alloy	Structure	B_s (T)	μ_e at 1 kHz	Core loss* (W / kg)	$\lambda_s \times 10^6$	D (nm)
$Fe_{84}Nb_{3.5}Zr_{3.5}B_8Cu_1$	mainly bcc	1.53	100000	0.06	0.3	8
$Fe_{84}Nb_7B_9$	mainly bcc	1.59	50000	0.10	0.2	9
$Fe_{90}Zr_7B_3$	mainly bcc	1.70	29000	0.17	-1.1	15
$Fe_{83}Nb_7B_9Cu_1$	mainly bcc	1.52	57000		1.1	8
$Fe_{89}Zr_7B_3Cu_1$	mainly bcc	1.60	35000		-1.1	11
Oriented Si-steel**	Ordered bcc	1.80	2400	0.73		
$Fe_{78}Si_9B_{13}$	Amorphous	1.56	9000	0.20	27	
$Fe_{73.5}Si_{13.5}B_9Nb_3Cu_1$**	mainly bcc	1.24	100000		2.1	12

* : f = 50 Hz, B_m = 1.4 T

** : Ref. [11]

[1] Y. Yoshizawa, S. Oguma and K. Yamauchi: J. Appl. Phys. **64** (1988) 6044.

[2] Y. Fujii, H. Fujita, A. Seki and T. Tomida: J. Appl. Phys. **70** (1991) 6241

[3] K. Suzuki, N. Kataoka, A. Inoue, A. Makino and T. Masumoto: Mater. Trans., JIM **31** (1990) 743.

[4] K. Suzuki, A. Makino, N. Kataoka, A. Inoue, and T. Masumoto: Mater. Trans., JIM **32** (1991) 93.

[5] K. Suzuki, A. Makino, A. Inoue, and T. Masumoto: J. Appl. Phys., **70** (1991) 6232.

[6] K. Suzuki, A. Makino, A. Inoue and T. Masumoto: Sci. Rep. RITU, **A39** (1994) 133.

[7] G. Herzer: IEEE Trans. Magn. **25** (1989) 3327.

[8] K. Suzuki, A. Makino, A. Inoue and T. Masumoto: J. Jpn. Inst. Metals **57** (1993) 964. (in Japanese)

[9] J. Kanamori: *Magnetism* (*Baifukan, Tokyo*, 1969) 102. (in Japanese)

[10]S. N. Kaul: J. Magn. Magn. Mater., **53** (1985) 5.

[11] Y. Yoshizawa and K. Yamauchi: J. Mag. Soc. Jpn., **13** (1989) 231.(in Japanese)